Benign and Malignant Part-Solid Nodules: Differentiation Via Thin-Section Computed Tomography

Zhi-gang Chu (chuzg0815@163.com)
First Affiliated Hospital of Chongqing Medical University
Wang-jia Li
First Affiliated Hospital of Chongqing Medical University
Fa-jin Lv
First Affiliated Hospital of Chongqing Medical University
Yi-wen Tan
First Affiliated Hospital of Chongqing Medical University
Bing-jie Fu
First Affiliated Hospital of Chongqing Medical University

Research Article

Keywords: Part-solid nodules, CT, Malignancy, Benignity, Solid component

Posted Date: January 19th, 2021

DOI: https://doi.org/10.21203/rs.3.rs-138228/v1

Abstract

Background: Pulmonary part-solid nodules (PSNs) are reported to have a high possibility of malignancy, while benign PSNs are not rare. This study aimed to reveal the differences between benign and malignant PSNs by comparing their thin-section CT features.

Methods: Patients with PSNs confirmed by postoperative pathological examination or follow-up (at the same period) were retrospectively enrolled from March 2016 to January 2020. The clinical data of patients and CT features of benign and malignant PSNs were reviewed and compared. The binary logistic regression analysis was performed to reveal predictors of malignant PSNs.

Results: A total of 119 PSNs in 117 patients (mean age, 56 years ± 11 [standard deviation]; 70 women) were evaluated. Of the 119 PSNs, 44 (37.0%) were benign, and 75 (63.0%) were malignant (12 adenocarcinomas in situ, 22 minimally invasive adenocarcinomas, and 41 invasive adenocarcinomas). Between benign and malignant PSNs, there were significant differences in patients' age and smoking history. Regarding CT characteristics, malignant lesions and benign lesions significantly differed in CT features of whole nodule, internal solid component, and peripheral ground-glass opacity. The binary logistic regression analysis revealed that well-defined border (odds ratio [OR], 4.574; 95% confidence interval [CI], 1.186-17.643; P=0.027) and lobulation (OR, 61.739; 95% CI, 5.230-728.860; P=0.001) of nodule, and irregular shape (OR, 9.502; 95% CI, 1.788-50.482; P=0.008) and scattered distribution (OR, 13.238; 95% CI, 1.359-128.924; P=0.026) of internal solid components were significant independent predictors distinguishing malignant PSNs.

Conclusions: Well-defined and lobulated PSNs with irregular and scattered solid components have a high probability of being malignant.

Background

With the widespread application of CT screening for lung cancer, the increasing detection of ground-glass nodules (GGNs) attracts attention because of their high possibility of being early lung cancer [1–4]. GGNs, based on the absence or presence of a solid component, can be further classified into pure GGNs and part-solid nodules (PSNs) [5]. PSN has been reported to be associated with lung adenocarcinoma, and its malignant rate is higher than that of pure GGNs and solid nodules [6, 7]. Pathologically, PSNs were mainly confirmed as minimally invasive adenocarcinoma and invasive adenocarcinoma, while pure GGNs were mostly adenocarcinoma in situ and sometimes minimally adenocarcinoma [8]. Therefore, an aggressive approach to treatment is usually recommended for PSNs, especially for lesions with solid components larger than 5 mm [5].

However, PSN is a nonspecific radiological manifestation, which could also be found in various benign conditions, such as inflammatory disease, focal interstitial fibrosis, or alveolar hemorrhage [9, 10]. And some of them could be spontaneously resolved during follow-up. Oh et al. [11] found that a significant portion (48.7%) of PSNs disappeared over follow-up, and most of them were resolved within 3 months

after initial detection. Therefore, quite a few PSNs could be benign lesions (BLs), and it is important to differentiate BLs from malignant lesions (MLs) based on initial CT data for the further management of PSNs.

Previous studies have investigated the differences in CT features of PSNs with different natures [11–13]. Yang et al. [12] reported that large size, well-defined border, and spiculation favored the diagnosis of MLs, and Lee et al. [13] revealed that lesion multiplicity, large solid component, and ill-defined lesion border indicated transient lesions. Although the differences in size and CT value of internal solid component were also studied [12, 13], these studies mainly compared the overall CT features of nodules rather than comprehensively analyzed the differences between their various components. What's more, some results were acquired based on the enrolled cases confirmed only by follow-up, which limited the clinical value of their findings. The current study enrolled patients with benign PSNs confirmed by follow-up or pathology and malignant lesions by pathology, and the CT features of whole nodule, internal solid component and peripheral GGO component were analyzed and compared, respectively. The results may provide more information for differentiating benign and malignant PSNs.

Methods

Study Population

From March 2016 to January 2020, patients with pathologically confirmed benign GGNs or resolved GGNs were collected, and cases with pathologically confirmed malignant GGNs during the same period were also collected. Then cases that met the following criteria were enrolled in this study. Inclusion criteria: (1) patients with pulmonary GGNs manifesting as PSNs; (2) patients' clinical data were complete. Exclusion criteria: (1) CT images with the thickness more than 1 mm; (2) presence of artifacts on CT images affecting evaluation. Finally, 117 patients with 119 PSNs were included in this study. The patients' selection procedure was shown in Fig. 1.

CT examinations

All patients underwent non-contrast chest CT with a 128-slice multi-detector CT scanner (SOMATOM Definition Flash system, Siemens Medical Systems) while holding their breath after inspiration, and were scanned from thoracic inlet to lung base. CT examinations were performed with the following parameters: tube voltage, 110 – 120 kV; tube current, 50 – 150 mAs; beam pitch, 1.0; detector collimation, 0.6 mm; rotation time, 0.5 s; reconstruction thickness, 1.0 mm or 0.625 mm; reconstruction interval, 1.0 mm or 0.625 mm, and reconstruction kernel, medium-sharp algorithm.

Analysis of CT Features

CT images of all patients were reviewed by two radiologists with more than ten-year experience of chest CT interpretation, who were blinded to clinical data and pathological results. Any divergences of the two radiologists during evaluation were resolved by consensus. CT images were analyzed with lung window

setting (window level, -600 HU; width, 1600 HU) by using Picture Archiving and Communication System and multiplanar reconstruction.

The overall CT features of each PSN were evaluated: *(a)* lesion size (mean of the longest diameter and the perpendicular diameter on axial images), *(b)* lesion area (the largest area of entire PSN on axial images), *(c)* location, *(d)* lesion shape (round, oval, or irregular), *(e)* lesion border (well-defined or ill-defined), *(f)* lesion margin (smooth or coarse), *(g)* lobulation, *(h)* spiculation, *(i)* air bronchogram, *(j)* bubble lucency, *(k)* pleural indentation, *(l)* pulmonary vessel changes (distorted, dilated, or both). For GGO component, its density and uniformity (homogeneous or heterogeneous) were also evaluated. CT features that were analyzed for solid component included *(a)* area (the largest area of internal solid component on axial images), *(b)* solid ratio (largest area of solid component divided by largest lesion area), *(c)* density, *(d)* number (solitary or multiple), *(e)* shape (round, oval, or irregular), *(f)* border (well-defined or ill-defined), *(g)* margin of well-defined solid component (smooth or coarse), *(h)* distribution (concentrated or scattered), *(i)* location (central, eccentric). We did not record the size for multiple and irregular solid components because it would preclude reliable and accurate evaluation.

Clinical and pathological data

Patients' clinical and laboratory data were recorded through Electronic Medical Record System. Clinical data, including patient age, sex, smoking history (never-smoker, ex-smoker, or current smoker), smoking amount and history of cancer were recorded. Laboratory findings, such as white blood cell (WBC) count, blood eosinophil count, and presence of blood eosinophilia, were also recorded. These laboratory examinations were performed before operation and within a week after CT examination.

All existing histopathologic slides were reviewed by two pathologists and histopathologic analysis was performed according to the 2015 World Health Organization classification of tumors of the lung, pleura, thymus, and heart [14].

Statistical Analysis

Continuous data are expressed as mean ± standard deviation, whereas categorical variables are presented as numbers and percentages. Continuous data were analyzed by using the analysis of Variance or Wilcoxon rank sum test, and categorical data were analyzed by Pearson χ^2 test or Fisher's exact test. A *P* value less than .05 was considered to indicate a statistically significant difference. All statistical analyses were performed by using SPSS 20.0 (SPSS, Chicago, Ill).

Binary logistic regression analysis was performed to identify variables that could be used in differentiating benign from malignant PSNs. Because of multi-collinearity in some clinical data and CT features, the least absolute shrinkage and selection operator (LASSO) was used to further select features. Characteristics with a *P* value of less than .05 at univariate analysis were used as the independent variables for LASSO analysis, and then the selected variables were put into binary logistic regression

analysis. Receiver operating characteristic analyses were conducted for the variables with statistically significant differences on logistic regression analysis.

Ethics

The study protocol was reviewed and approved by the Ethics Committee of The First affiliated Hospital of Chongqing Medical University (IRB No: 2019-062). The recommendations of the Declaration of Helsinki for biomedical research involving human subjects were also followed.

Results

Clinical features

One hundred and seventeen patients (mean age, 56 years ± 11; age range, 24 –79 years) were enrolled in this study. Of the 117 patients, 70 (59.8%) were women (mean age, 56 years ± 11; age range, 29 – 84 years), and 47 (40.2%) were men (mean age, 55 years ± 11; age range, 25 – 76 years). Thirty-one (31/117, 26.5%) patients had a history of smoking with the mean number of 26 pack-years (range, 0.8 – 80 pack-years) and 10 (8.5%) patients had a history of cancer. Only two patients had blood eosinophilia and were diagnosed with benign nodules.

The clinical data of 117 patients with BLs and MLs were summarized in Table 1. Among 117 patients with 119 PSNs, there were 73 (62.4%) patients with 75 (63.0%) MLs, including 12 (16.0%) adenocarcinomas in situ (AISs), 22 (29.3%) minimally invasive adenocarcinomas (MIAs), and 41 (54.7%) invasive adenocarcinomas (IAs). Of 44 (37.6%) patients with 44 (37.0%) BLs, 17 (38.6%) were completely resolved during follow-up and 27 (61.4%) were confirmed by postoperative pathologic examination. The patients with MLs were older than patients with BLs (P=0.005), and most of them were nonsmokers (P=0.005).

CT features of benign and malignant PSNs

The overall CT findings of benign and malignant PSNs were showed in Table 2. The MLs were significantly larger than BLs (P<0.001), and were more likely to have well-defined border (P<0.001) and heterogeneous GGO (P=0.004). Regarding the morphological features, MLs showed lobulation (P<0.001), bubble lucency (P=0.001) and pleural indentation (P<0.001) more frequently than did BLs (Fig. 2). And all PSNs with spiculation, air bronchogram and pulmonary vessel changes were MLs.

The CT findings of solid components in BLs and MLs were summarized in Table 3. The solid components in MLs were significantly larger than those in BLs (P < .001), and were more likely to be multiple (P<0.001), irregular (P<0.001), scattered (P<0.001) and eccentric (P=0.008) (Fig. 2, Fig. 3). While solid components in BLs were usually single, round, and central (Fig. 4) and were more likely to be ill-defined (P<0.001).

Binary logistic regression analysis revealed that well-defined border (odds ratio [OR], 4.574; 95% confidence interval [CI], 1.186-17.643; P=0.027) and lobulation (OR, 61.739; 95% CI, 5.230-728.860; P<0.001) of lesion, irregular shape (OR, 9.502; 95% CI, 1.788-50.482; P=0.008) and scattered distribution (OR, 13.238; 95% CI, 1.359-128.924; P=0.026) of solid components were significant predictors distinguishing malignant PSNs. Receiver operating characteristic analysis revealed that the areas under the curve for the border and lobulation of nodule, and shape and distribution of solid components were 0.710 (95% CI, 0.613-0.808; P<0.001), 0.775 (95% CI, 0.691- 0.858; P<0.001), 0.737 (95% CI, 0.638- 0.837; P<0.001), and 0.731 (95% CI, 0.642- 0.820; P<0..001), respectively (Fig. 5).

Discussion

Most PSNs are confirmed as MLs with invasiveness, but there are still some benign PSNs and some of them could disappear spontaneously [15]. As for treatment, BLs just require follow up, while MLs need early surgical resection [16]. Therefore, it is important to differentiate benign from malignant PSNs. This study investigated the clinical data of patients and CT features of benign and malignant PSNs, especially the differences of solid components. It was found that patients with MLs were more likely to be older and nonsmokers, and BLs and MLs significantly differed in CT features of whole nodule, internal solid component and GGO. In summarize, well-defined border and lobulation of nodule, and irregular shape and scattered distribution of internal solid components were significant indicators of malignant PSNs.

Most previous studies [17-20] mainly investigated the overall CT features of benign and malignant GGNs, and found significant differences in lesion size, border, lobulation spiculation, bubble lucency, air bronchogram, vascular convergence sign, and pleural indentation between BLs and MLs. In addition, some researches [11, 12] investigated the overall CT features of BLs and MLs appearing as PSNs. Oh et al. [11] analyzed 86 histologically confirmed or transient PSNs (29 malignant and 57 transient lesions), and found that MLs were more likely to be larger and have spiculation than BLs. According to Yang et al. [12] a larger size, well-defined border, and spiculation had higher predictive value for malignant PSNs. Although there are some differences among these studies because of different inclusion criteria, most of present findings are consistent with the previous results.

Compared with pure GGNs, the solid components in PSNs make them more characteristic. Therefore, it deserves to be meticulously analyzed and may provide additional findings for differential diagnosis of BLs and MLs. Previous researches [12,13,18,21] only investigated the size or/and CT value of solid component. Yang et al. [12] found that MLs were more likely to have a larger solid component with higher CT value than BLs, but its morphological manifestations were not well studied. The present study conducted a comprehensive analysis of solid component, and revealed that PSNs with larger, irregular, multiple, scattered, and eccentric solid components had a higher probability of malignancy, while BLs usually had single, round, and ill-defined solid components. However, there was no significant difference in density between MLs and BLs. In addition to the size and CT value of solid component, the current study found more characteristics with predictive value, which could provide new information for more

accurate diagnosis. Therefore, solid component is an important part of PSN and has great significance in diagnosis.

Pathologically, solid components in MLs were confirmed as tumor invasion with or without alveolar collapse or/and fibroblastic proliferation [22]. Different cell differentiation degrees and growth rates result in irregular shape of solid components, and the multiple scattered solid components may be related to multiple origins of invasions. Regarding benign PSNs, most of them were inflammatory lesions. The internal solid components usually represent a large number of inflammatory cells, and GGO represents exudates and fibrotic changes [1]. This indicates that inflammation in solid component is more severe than that in peripheral GGO, and the peripheral GGO might be secondary to central inflammation. Thus, in benign PSNs, the border of solid component and its peripheral GGO were usually ill-defined.

Our study had two limitations. First, the sample size of benign PSNs is small. Therefore, more cases are needed in future studies to confirm our results' accuracy. Second, variations in nodule measurement and characterization of lesions might exist due to different radiologists. Thus, we measured relevant parameters for three times and evaluated CT features of PSNs using multiplanar reconstruction. The consistent results of radiologists were used to ensure the reliability of results.

Conclusions

Benign and malignant PSNs had significant differences in CT features. Well-defined and lobulated PSNs with irregular, multiple, and scattered solid components have a high probability of being malignant. In contrast, PSNs with sole, round, and blurred solid component indicate benign lesions, and follow-up should be firstly considered for them.

Abbreviations

PSN: Part-solid nodule; GGN: Ground-glass nodule; BL: Benign lesion; ML: Malignant lesion; GGO: Ground-glass opacity; OR: Odds ratio; CI: Confidence interval; ROC: Receiver operating characteristic; WBC: White blood cell.

Declarations

Ethics approval and consent to participate: This retrospective study was approved by the medical ethical committee of the First Affiliated Hospital of Chongqing Medical University and the requirement for informed consent was waived.

Consent for publication: Not applicable.

Availability of data and materials: The datasets used and/or analyzed during the current study are available from the corresponding author on reasonable request.

Competing interests: The authors declare that they have no competing interests.

Funding: This work was supported by the National Natural Science Foundation of China (81601545) and Chongqing Health and Family Planning Commission Foundation (2016MSXM018) of China.

Author contributions: CZG designed the study, reviewed and edited the manuscript. WJL and FJL participated in data interpretation and writing-original draft preparation. YWT and BJF contributed to the statistical analysis. All authors have approved the final version of the work.

Acknowledgments: Not applicable.

Author information

[1]Department of Radiology, The First Affiliated Hospital of Chongqing Medical University, 1# Youyi Road, Yuanjiagang, Yuzhong district, Chongqing, 400016, People's Republic of China.

Wang-jia Li, Fa-jin Lv, Bin-jie Fu, Zhi-gang Chu.

[2]Department of Pathology, The First Affiliated Hospital of Chongqing Medical University, 1# Youyi Road, Yuanjiagang, Yuzhong district, Chongqing, 400016, People's Republic of China.

References

1. Park CM, Goo JM, Lee HJ, Lee CH, Chun EJ, Im JG. Nodular ground-glass opacity at thin-section CT: histologic correlation and evaluation of change at follow-up. Radiographics. 2007,27(2):391-408.
2. Mao R, She Y, Zhu E, Chen D, Dai C, Wu C, et al. Proposal for Restaging of Invasive Lung Adenocarcinoma Manifesting as Pure Ground Glass Opacity. Ann Thorac Surg. 2019,107(5):1523-1531.
3. She Y, Zhao L, Dai C, Chen Y, Zha J, Xie H, et al. Preoperative nomogram for identifying invasive pulmonary adenocarcinoma in patients with pure ground-glass nodule: A multi-institutional study. Oncotarget. 2017,8(10):17229-17238.
4. Kim HY, Shim YM, Lee KS, Han J, Yi CA, Kim YK. Persistent pulmonary nodular ground-glass opacity at thin-section CT: histopathologic comparisons. Radiology. 2007,245(1):267-275.
5. Naidich DP, Bankier AA, MacMahon H, Schaefer-Prokop CM, Massimo Pistolesi M, Goo JM, et al. Recommendations for the management of subsolid pulmonary nodules detected at CT: a statement from the Fleischner Society. Radiology. 2013,266(1):304-17.
6. Lee HJ, Goo JM, Lee CH, Yoo CG, Kim YT, Im JG. Nodular ground-glass opacities on thin-section CT: size change during follow-up and pathological results. Korean J Radiol. 2007,8(1):22-31.
7. Henschke CI, Yankelevitz DF, Mirtcheva R, McGuinness G, McCauley D, Miettinen OS, et al. CT screening for lung cancer: frequency and significance of part-solid and nonsolid nodules. AJR Am J Roentgenol. 2002,178(5):1053-1057.

8. Ye T, Deng L, Wang S; Chen H, Zhang Y, Hu W, et al. Lung Adenocarcinomas Manifesting as Radiological Part-Solid Nodules Define a Special Clinical Subtype. J Thorac Oncol. 2019,14(4):617-627.
9. Nagajima R, Yokose T, Kakinuma R, Nagi K, Nishiwaki Y, Ochiai A. Localized pure ground-glass opacity on highresolution CT: histologic characteristics. J Comput Assist Tomogr. 2002,26:323-9.
10. Yamada N, Kusumoto M, Maeshima A, Suzuki K, Matsuno Y. Correlation of the solid part on high-resolution computed tomography with pathological scar in small lung adenocarcinomas. Jpn Clin Oncol. 2007,37(12):913-7.
11. Oh JY, Kwon SY, Yoon HI, Lee SM, Yim JJ, Lee JH, et al. Clinical significance of a solitary ground-glass opacity (GGO) lesion of the lung detected by chest CT. Lung Cancer. 2007,55(1):67-73.
12. Yang W, Sun Y, Fang W, Qian F, Ye J, Chen Q, et al. High-resolution Computed Tomography Features Distinguishing Benign and Malignant Lesions Manifesting as Persistent Solitary Subsolid Nodules. Clin Lung Cancer. 2018,19(1):e75-e83.
13. Lee SM, Park CM, Goo JM, Lee CH, Lee HJ, Kim KG, et al. Transient Part-Solid Nodules Detected at Screening Thin-Section CT for Lung Cancer: Comparison with Persistent Part-Solid Nodules. Radiology. 2010,255(1):242-51.
14. Travis WD, Brambilla E, Burke AP, Marx A, Nicholson AG. Introduction to the 2015 World Health Organization classification of tumors of the lung, pleura, thymus, and heart. J Thorac Oncol. 2015,10:1240-2.
15. Choi WS, Park CM, Song YS, Lee SM, Wi JY, Goo JM. Transient subsolid nodules in patients with extrapulmonary malignancies: their frequency and differential features. Acta Radiol. 2015,56:428-437.
16. Pedersen JH, Saghir Z, Wille MM, Thomsen LH, Skov BG, Ashraf H. Ground-Glass Opacity Lung Nodules in the Era of Lung Cancer CT Screening: Radiology, Pathology, and Clinical Management. Oncology (Williston Park). 2016,30(3):266-74.
17. Fan L, Liu SY, Li QC, Yu H, Xiao XS. Multidetector CT features of pulmonary focal ground-glass opacity: differences between benign and malignant. Br J Radiol. 2012,85(1015):897-904.
18. Hu H, Wang Q, Tang H, Xiong L, Lin Q. Multi-slice computed tomography characteristics of solitary pulmonary ground-glass nodules: Differences between malignant and benign. Thorac Cancer. 2016,7(1):80-7.
19. Gao F, Sun Y, Zhang G, Zheng X, Li M, Hua Y. CT characterization of different pathological types of sub-centimeter pulmonary ground-glass nodular lesions. Br J Radiol. 2019,92(1094):20180204.
20. Qiu ZX, Cheng Y, Liu D, Wang WY, Wu X, Wu WL, et al. Clinical, pathological, and radiological characteristics of solitary ground-glass opacity lung nodules on high-resolution computed tomography. Ther Clin Risk Manag. 2016,12:1445-1453.
21. Chen ML, Li XT, Wei YY, Qi LP, Sun YS. Can spectral computed tomography imaging improve the differentiation between malignant and benign pulmonary lesions manifesting as solitary pure ground glass, mixed ground glass, and solid nodules? Thorac Cancer. 2019,10(2):234-242.

22. Lee HJ, Lee CH, Jeong YJ, et al. IASLC/ATS/ERS international multidisciplinary classification of lung adenocarcinoma: novel concepts and radiologic implications. J Thorac Imaging. 2012,27(6):340-53.

Tables

Table1. Clinical features of 117 patients

Clinical features	Patients with Benign PSNs (n=44)	Patients with Malignant PSNs (n=73)	*P* Value
Age (y)	52 ± 11	58 ± 11	0.005*
Sex			
Male	21 (47.7)	26 (35.6)	0.196‡
Female	23 (52.3)	47 (64.4)	
Smoking history			
Never-smoker	25 (56.8)	61 (83.6)	
Ex-smoker	5 (11.4)	3 (4.1)	0.005§
Current smoker	14 (31.8)	9 (12.3)	
Smoking amount (pack-years)	23 ± 20	27 ± 16	0.404&
History of cancer			
Present	2 (4.5)	8 (11.0)	0.316§
Absent	42 (95.5)	65 (89.0)	
WBC count (uL^{-1})	6872 ± 2931	5631 ± 2214	0.051§
Blood eosinophil count (uL^{-1})	154 ± 223	100 ± 92	0.930§
Blood eosinophilia			
≥500 per microlite	2 (4.5)	0 (0.0)	0.139§
<500 per microliter	42 (95.5)	73 (100.0)	

Note. Data are presented as n (%) or Means ± SD.

* Analysis of Variance, ANOVA.

‡ Calculated with the Pearson χ^2 test.

§ Calculated with the Fisher exact test.

& Wilcoxon rank sum test.

Table2. The overall CT findings of benign and malignant PSNs

CT features	Benign PSNs (n=44)	Malignant PSNs (n=75)	*P* Value
Lesion size (mm)	11.1 ± 4.3	15.2 ± 4.8	<0.001*
Lesion area (mm^2)	118.4 ± 89.8	199.4 ± 116.8	<0.001&
Density of GGO (HU)	-635 ± 84	-616 ± 81	0.241*
Location			
Right upper lobe	16 (36.4)	33 (44.0)	
Right middle lobe	1 (2.3)	2 (2.7)	
Right lower lobe	7 (15.9)	6 (8.0)	0.528§
Left upper lobe	12 (27.3)	25 (33.3)	
Left lower lobe	8 (18.2)	9 (12.0)	
Lesion shape			
Round/Oval	13 (29.5)	17 (22.7)	0.404‡
Irregular	31 (70.5)	58 (77.3)	
Lesion border			
Well-defined	12 (27.3)	52 (69.3)	<0.001‡
Ill-defined	32 (72.7)	23 (30.7)	
Margin of well-defined border			
Smooth	3 (25.0)	5 (9.6)	0.164§
Coarse	9 (75.0)	47 (90.4)	
Uniformity of GGO			
Homogeneous	28 (63.6)	27 (36.0)	0.004‡
Heterogeneous	16 (36.4)	48 (64.0)	
Lobulation	2 (4.5)	45 (60.0)	<0.001‡
Spiculation	0 (0.0)	22 (29.3)	<0.001‡
Air bronchogram	0 (0.0)	18 (24.0)	<0.001‡
Bubble lucency	1 (2.3)	19 (25.3)	0.001‡
Pleural indentation	3 (6.8)	35 (46.7)	<0.001‡

Pulmonary vessel changes	0 (0.0)	33 (44.0)	0.001‡

Note. Data are presented as n (%) or Means ± SD.

* Analysis of Variance, ANOVA.

‡ Calculated with the Pearson χ^2 test.

§ Calculated with the Fisher exact test.

& Wilcoxon rank sum test.

Table3. The CT findings of solid component within Benign and Malignant PSNs

CT features	Patients with Benign PSNs (n=44)	Patients with Malignant PSNs (n=75)	*P* Value
Solid component area* (mm^2)	15.6 ± 15.0	34.6 ± 30.5	<0.001[&]
Solid component radio* (%)	12.4 ± 7.6	16.8 ± 9.6	0.015[&]
Density of Solid component*	-164 ± 196	-99 ± 130	0.155[&]
Solid component number			
Solitary	41 (93.2)	34 (45.3)	<0.001[‡]
Multiple	3 (6.8)	41 (54.7)	
Solid component shape			
Round	25 (56.8)	7 (9.3)	<0.001[‡]
Irregular	19 (43.2)	68 (90.7)	
Solid component border			
Well-defined	6 (13.6)	35 (46.7)	<0.001[‡]
Ill-defined	38 (86.4)	40 (53.3)	
margin of well-defined solid component			
Smooth	6 (100.0)	11 (31.4)	0.003[§]
Coarse	0 (0.0)	24 (68.6)	
Solid component distribution			
Concentrated	42 (95.5)	37 (49.3)	<0.001[‡]
Scattered	2 (4.5)	38 (50.7)	
Solid component location			
Central	21 (47.7)	18 (24.0)	0.008[‡]
Eccentric	23 (52.3)	57 (76.0)	

Note: Data are presented as n (%) or Means ± SD.

[‡] Calculated with the Pearson χ^2 test.

§ Calculated with the Fisher exact test.

[&] Wilcoxon rank sum test.

Figures

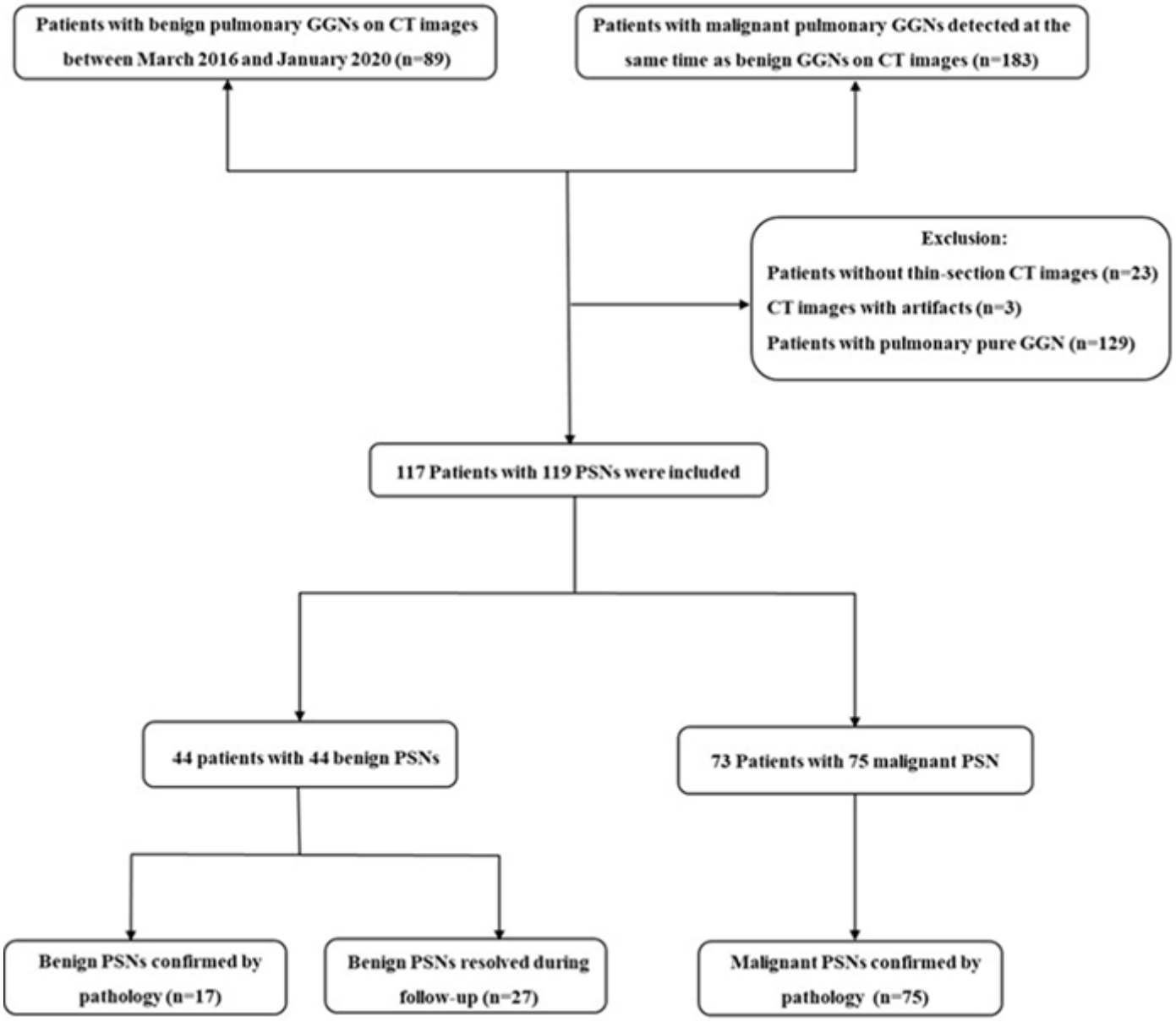

Figure 1

Flowchart of study population

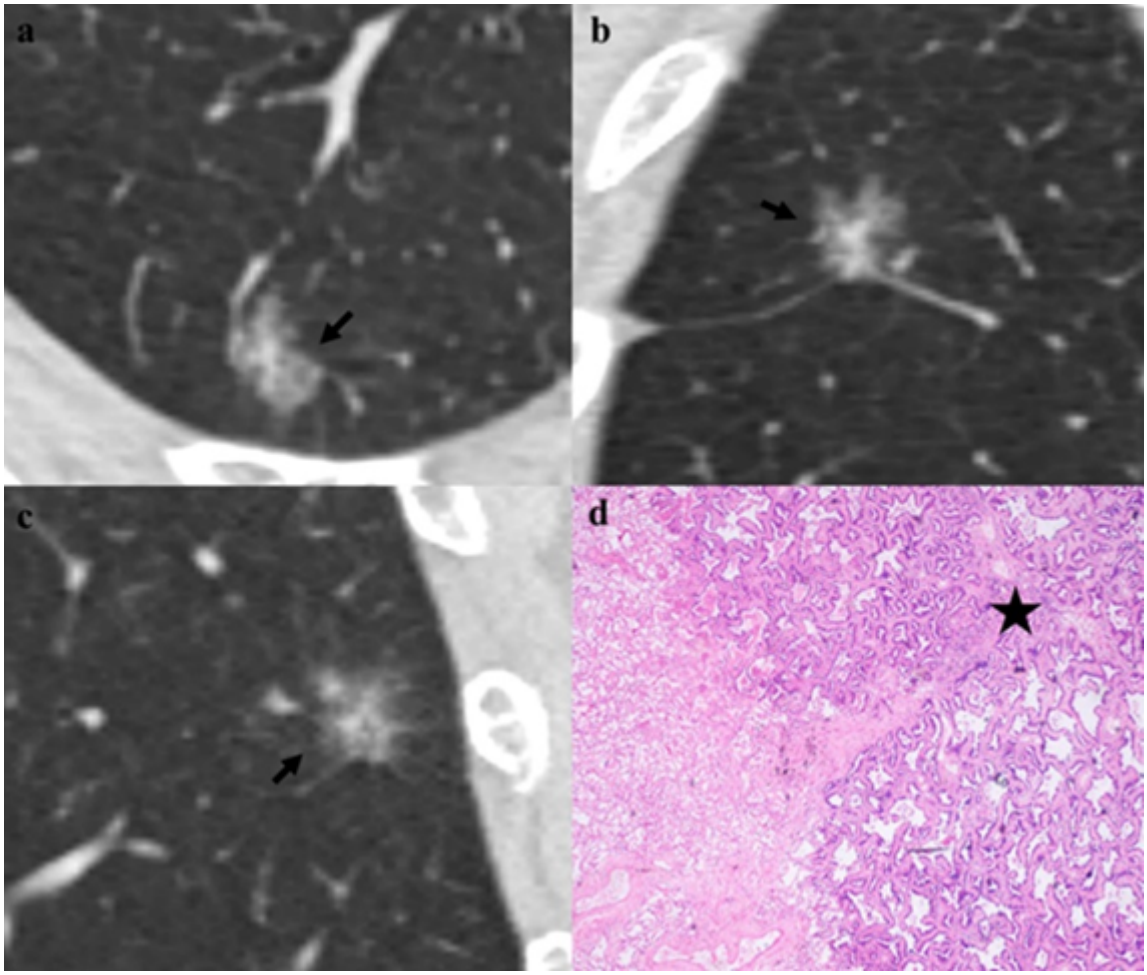

Figure 2

A 55-year-old woman with an invasive adenocarcinoma. Axial (a), coronal (b) and sagittal (c) CT images show a 13-mm lobulated and well-defined PSN (arrows) in the right upper lobe. The internal solid components are multiple, scattered, and irregular, and the peripheral GGO is heterogeneous. (d) Photomicrograph (hematoxylin - eosin stain) of PSN reveals adenocarcinoma with invasive foci (asterisk).

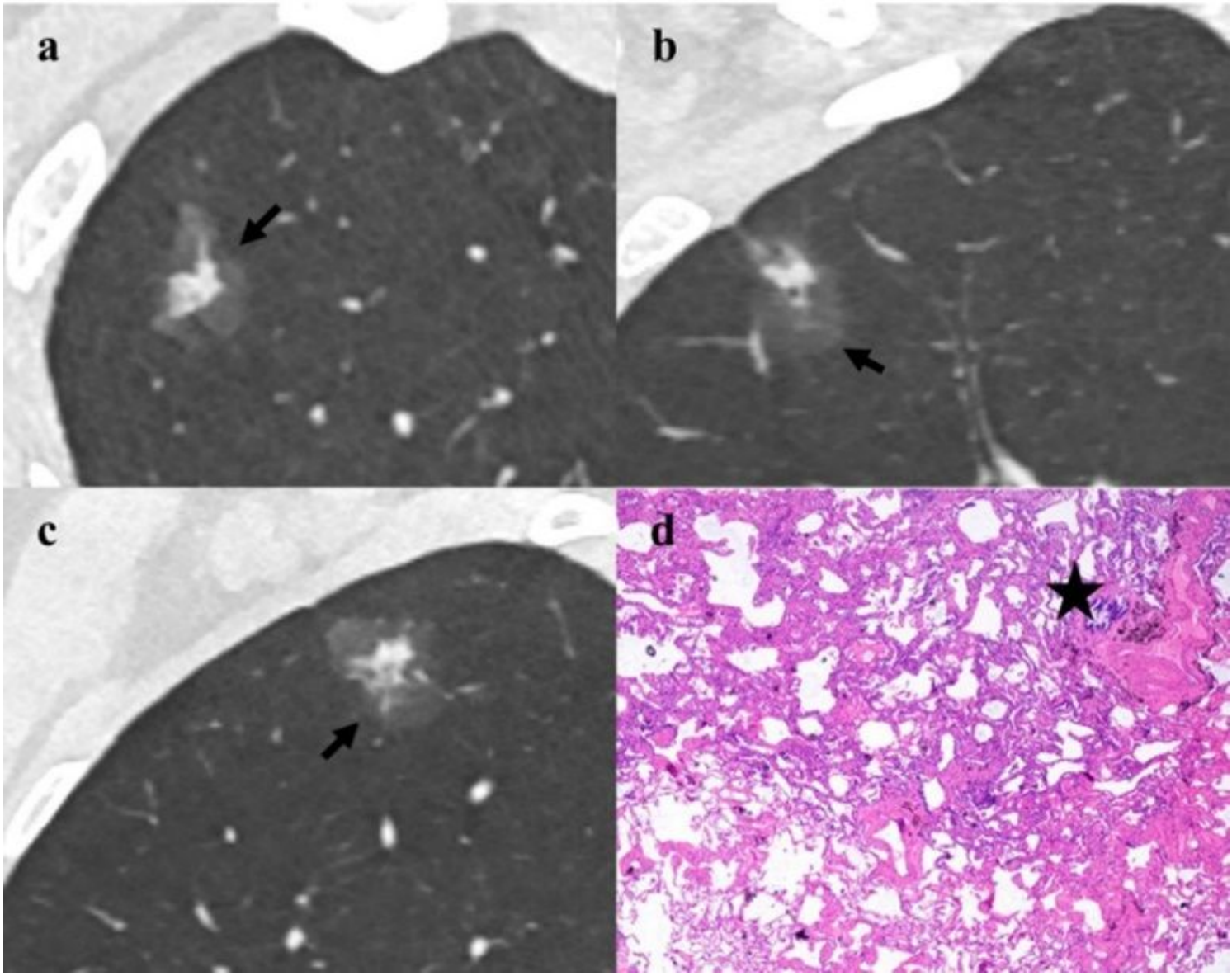

Figure 3

A 50-year-old woman with an invasive adenocarcinoma. Axial (a), coronal (b) and sagittal (c) CT images show a 17-mm irregular and well-defined PSN (arrows) in the right upper lobe, the internal solid component is eccentric, irregular, and well-defined, and the peripheral GGO is homogeneous. Photomicrograph (hematoxylin - eosin stain) of PSN reveals adenocarcinoma with invasive foci (asterisk).

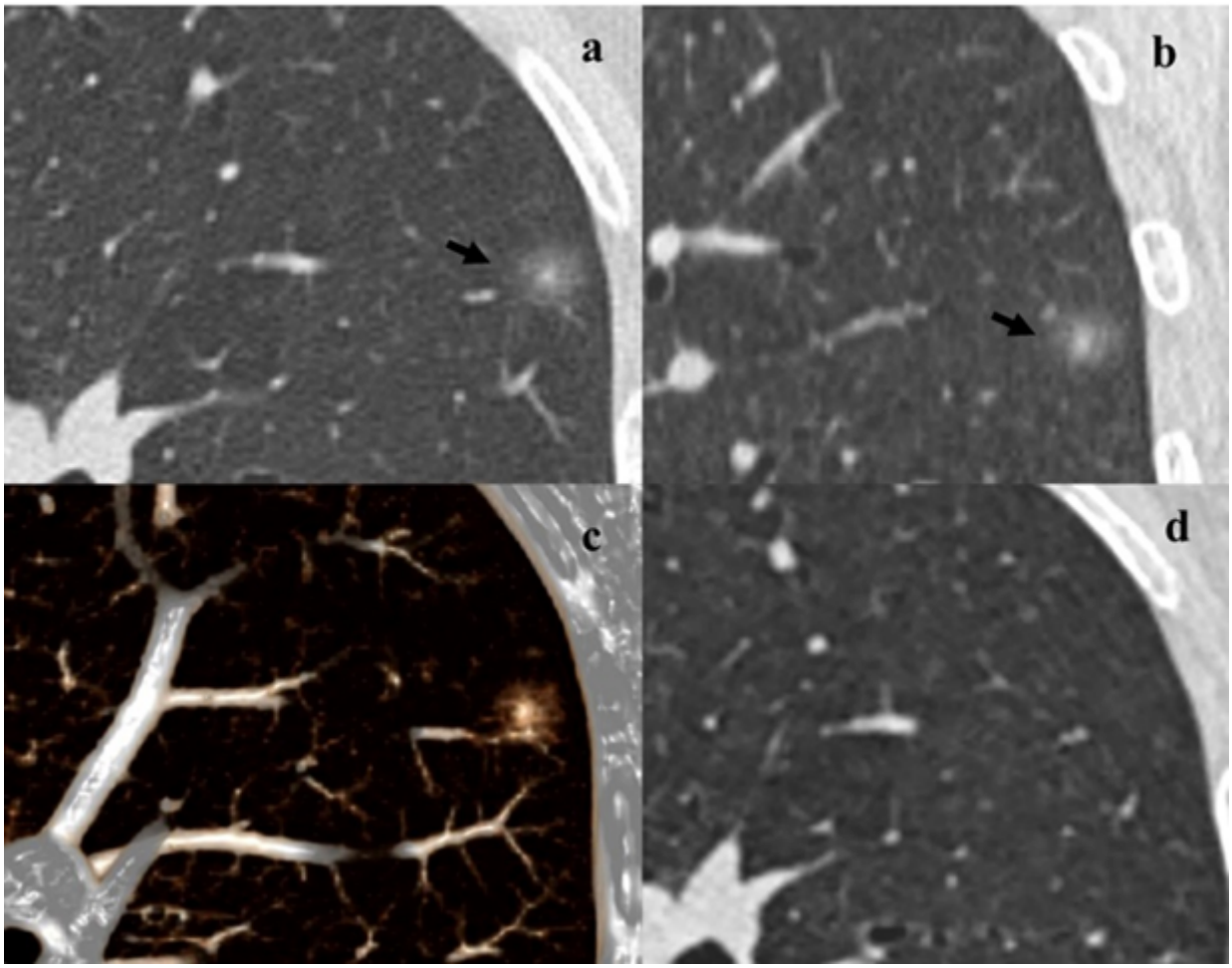

Figure 4

A 63-year-old woman with a transient PSN in the left upper lobe. Axial (a) and sagittal (b) CT images show an 8-mm round PSN (arrows), the internal high-attenuation zone is centric, round, and ill-defined, and the peripheral GGO is ill-defined. VR image (c). At follow-up CT (d) obtained 3 months later, the PSN has disappeared.

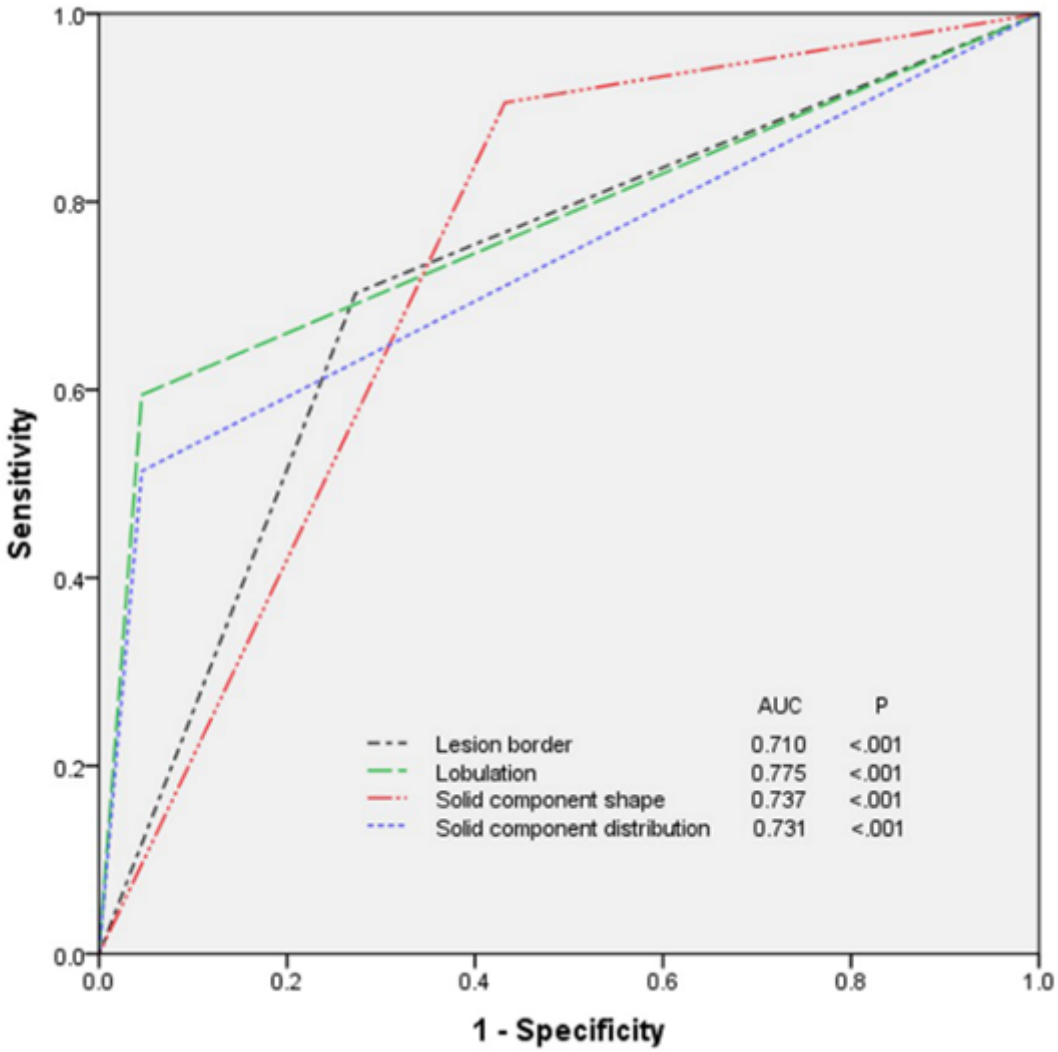

Figure 5

Receiver operating characteristic Curve for lesion border, lobulation, solid component shape and distribution in part-solid nodule.